Global and Planetary Change 216 (2022) 103891

Contents lists available at ScienceDirect

Global and Planetary Change

journal homepage: www.elsevier.com/locate/gloplacha

Early to middle Miocene ice sheet dynamics in the westernmost Ross Sea (Antarctica): Regional correlations

Lara F. Pérez [a,b,*], Robert M. McKay [c], Laura De Santis [d], Robert D. Larter [a], Richard H. Levy [c,e], Timothy R. Naish [c], John B. Anderson [f], Philip J. Bart [g], Martina Busetti [d], Gavin Dunbar [c], Chiara Sauli [d], Christopher C. Sorlien [h], Marvin Speece [i]

[a] British Antarctic Survey, High Cross, Madingley Road, Cambridge CB3 0ET, UK
[b] Geological Survey of Denmark and Greenland, Department of Marine Geology, Aarhus University, University City 81, building 1872, 6 floor, DK-8000 Aarhus C, Denmark
[c] Antarctic Research Centre - Victoria University of Wellington, Cotton Building Gate 7, Kelburn Parade, Wellington, New Zealand
[d] National Institute of Oceanography and Applied Geophysics, Borgo Grotta Gigante 42/C, 34010 Sgonico, Trieste, Italy
[e] GNS Science, 1 Fairway Drive, Avalon 5010 PO Box 30-368, Lower Hutt 5040, New Zealand
[f] Rice University, 6100 Main St, Houston, TX 77005, United States
[g] Louisiana State University, Baton Rouge, LA 70803, United States
[h] University of California, UC Santa Barbara, Santa Barbara, California 93106, United States
[i] Montana Technological University, 1300 W Park St, Butte, MT 59701, United States

ARTICLE INFO

Editor: Dr. Alan Haywood

Keywords:
Miocene climatic optimum
Middle miocene climatic transition
Seismic correlation
West Antarctic ice sheet
East Antarctic ice sheet
Ice sheet evolution

ABSTRACT

The present-day morpho-stratigraphy of the Ross Sea is the result of Cenozoic tectonic and cryospheric events, and constitutes a key record of Antarctica's cryospheric evolution. An enduring problem in interpreting this record in a broader regional context is that the correlation between eastern and western Ross Sea stratigraphy has remained uncertain due to the limited number of drill sites. We correlate the glacial-related features observed on a dense network of seismic reflection profiles in McMurdo Sound with those identified in the Nordenskjöld and Drygalski Basins, as well as the basins farther east in the central Ross Sea. We present an improved correlation of the regional patterns of early to middle Miocene ice-sheet variance across the Ross Sea constrained by new evaluation of seismic facies and age models from one site recovered by the Antarctic Drilling Project (ANDRILL) in the southwestern most part of McMurdo Sound. We also integrate this correlation with the recently published seismic framework in the central Ross Sea. The formation of U-shaped valleys during the early Miocene in McMurdo Sound, together with prograding sedimentary wedges in the western-most basins, and the central Ross Sea, suggest two major phases of overall advance of a marine-terminating ice sheet between ~18 Ma and ~17.4 Ma. Widespread formation of turbiditic channel-levee systems in McMurdo Sound and rapid sediment deposition in Nordernskjöld Basin point to subsequent ice-sheet retreat between ~17.4 Ma and ~15.8 Ma, coinciding with the onset of the Miocene Climate Optimum (MCO; ~17–14.5 Ma). However, the carving of troughs and formation of irregular morphologic features suggest that an extensive ice sheet still remained along the western Ross margin at ~17.4 Ma and a brief episode of ice-sheet advance occurred at ~16.8 Ma in the earliest interval of the MCO. Subsequent marine-based ice sheet advance during the Middle Miocene Climate Transition (MMCT, ~14.0–13.8 Ma) is indicated by widespread erosional features. Our results reconcile the semi-continouous seismic and drill core stratigraphy of the offshore Ross Sea continental shelf with inferences of ice sheet dynamics from continuous far-field deep sea and sea level records, as well as the highly discontinous (and heavily debated) onshore records of pre-MMCT glaciation and aridification of the Transantarctic Mountains at 14 Ma.

* Corresponding author at: Geological Survey of Denmark and Greenland, Department of Marine Geology, Aarhus University, University City 81, building 1872, 6 floor, DK-8000 Aarhus C, Denmark.

E-mail addresses: lfp@geus.dk (L.F. Pérez), robert.mckay@vuw.ac.nz (R.M. McKay), ldesantis@ogs.it (L. De Santis), rdla@bas.ac.uk (R.D. Larter), R.Levy@gns.cri.nz (R.H. Levy), timothy.naish@vuw.ac.nz (T.R. Naish), johna@rice.edu (J.B. Anderson), pbart@lsu.edu (P.J. Bart), mbusetti@ogs.it (M. Busetti), gavin.dunbar@vuw.ac.nz (G. Dunbar), csauli@ogs.it (C. Sauli), christopher.sorlien@ucsb.edu (C.C. Sorlien), mspeece@mtech.edu (M. Speece).

https://doi.org/10.1016/j.gloplacha.2022.103891
Received 18 March 2022; Received in revised form 30 June 2022; Accepted 7 July 2022
Available online 9 July 2022

1. Introduction and background

Ice sheet advance and retreat over high-latitude continental shelves result in characteristic depositional and erosional features that enable the identification of major changes in the cryospheric evolution through time (e.g., Dowdeswell et al., 2016). When preserved in geophysical and geological records, dating these features allows the reconstruction of the past timing of changes in the ice sheet extent, which is critical to understanding the role of Antarctica in the global climate system.

The present-day morpho-stratigraphy of the Ross Sea (Fig. 1) has developed through a series of tectonic and cryospheric events since the Late Cretaceous. The broad Ross Sea continental shelf represents the extended lithosphere of the West Antarctic Rift between East and West Antarctica (Davey and Brancolini, 1995; Tinto et al., 2019). After Late Cretaceous continental breakup and subsidence (Eagles et al., 2004), slow thermal subsidence continued into the early Miocene (Fielding et al., 2008; Sauli et al., 2021), in addition to subsequent rifting phases related to the West Antarctic Rift extension (Cande et al., 2000; Granot and Dyment, 2018). Rifting, tilting and magmatic activity is still ongoing within the Terror Rift (e.g., Davey and Brancolini, 1995; Naish et al., 2007). Sediment erosion and transport by dynamic ice sheet systems have resulted in highly variable sediment supply through time (e.g., Naish et al., 2001; Levy et al., 2016; Anderson et al., 2019; Paxman et al., 2019; Marschalek et al., 2021; Pérez et al., 2021; McKay et al., 2022). The western margin of the Ross Sea is dominated by the topography of the Transantarctic Mountains where fluvial systems, together with the advance and retreat of the East Antarctic Ice Sheet (EAIS), have carved high-relief morphologies since at least the earliest Oligocene (e.g., Sugden and Denton, 2004; Levy et al., 2022). Offshore, marine-terminating EAIS outlet glaciers periodically extended across the westernmost Ross Sea during its Miocene evolution, with numerous large scale transient glacial advances noted in offshore drill core records (e.g., De Santis et al., 1995; Naish et al., 2001; Levy et al., 2016; Anderson et al., 2019). These ice sheet changes have been a primary driver of the stratigraphic architecture of the Antarctic margin and continental shelf basins.

The westernmost Ross Sea includes the McMurdo Sound and the Nordenskjöld and Drygalski Basins (Fig. 1), which contain sedimentary sequences that have been extensively studied through seismic records (Brancolini et al., 1995; De Santis et al., 1995; Bart and De Santis, 2012; Fielding et al., 2008; Pekar et al., 2013; Sauli et al., 2014, 2021). Results from several drilling projects in McMurdo Sound [i.e., the international Cenozoic Investigation in the Western Ross Sea project (CIROS, Barrett, 1989), the Cape Roberts Project (CRP; Fielding and Thomson, 1999) and the ANtarctic geological DRILLing (ANDRILL) project (Naish et al., 2007; Florindo et al., 2008)] provide lithologic and chronologic constraints for seismic interpretations. The westernmost basins are heavily influenced by the Neogene faulting and magmatism of the Terror Rift (e.g., Sauli et al., 2021). Their eastern margin is formed by the shallow depths of the Crary and Mawson banks and a chain of volcanic edifices in the surroundings of the modern Franklin, Beaufort and Ross Islands (Fig. 1). These volcanic edifices formed since the mid-Miocene (Wright and Kyle, 1990), combined with the tectonic complexity of the Ross Sea, have prevented direct correlation between the seismic sequences contained in the western, central and eastern sedimentary basins (Fig. 1).

In this work, we correlate the seismic features observed and dated in McMurdo Sound with those identified in the Nordenskjöld and Drygalski Basins, and extend these correlations to the central Ross Sea. Ultimately, we propose the first regional correlation of early to middle Miocene events between the western and central Ross Sea, informed by seismic facies and age constraints from a drill site recovered by ANDRILL in southern McMurdo Sound (Levy et al., 2016), as well as the

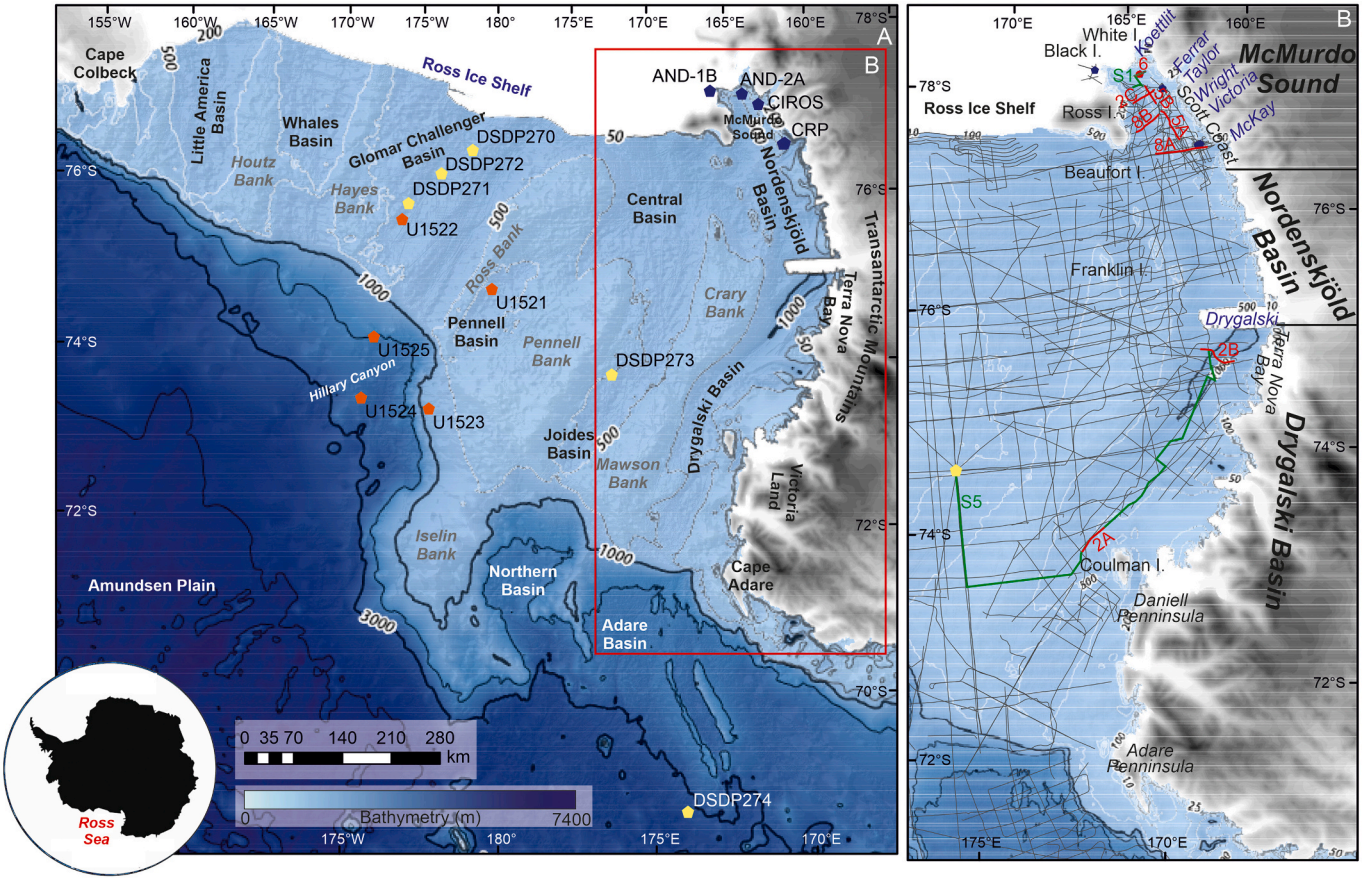

Fig. 1. A) Overview of the Ross Sea bathymetry (Arndt et al., 2013). Color dots represent legacy drill cores. B) Western Ross Sea continental shelf. Grey lines mark the location of seismic reflection profiles used in this work. The locations of the seismic profiles shown in the figures are highlighted.

International Ocean Drilling Program (IODP) Expedition 374 and Deep Sea Drilling Program (DSDP) Leg 28 sites in the central Ross Sea (McKay et al., 2019; Pérez et al., 2021; Marschalek et al., 2021). The ANDRILL Site AND-2A recovered a semi-continuous record of Miocene sediments (back to 20.5 Ma) in the inner part of McMurdo Sound (Florindo et al., 2008), while IODP Expedition 374 obtained records extending back to 18 Ma in the middle continental shelf of the Ross Sea. Age data from these sites provide chronostratigraphic constraints on the glacial-related features identified within the seismic stratigraphic framework across the Ross Sea to identify the regional variations in the glacial systems influencing the continental shelf through the Miocene (Fig. 1).

2. Methods

A broad network of multi- (MCS) and single-channel (SCS) reflection seismic profiles exist over the continental shelf of the Ross Sea, including the westernmost basins (Fig. 1). They were acquired by various national and international programs over several decades, and consequently data quality and resolution are variable. Most of the MCS lines are available in stack version at the SCAR Seismic Data Library System for Cooperative Research (SDLS) (https://sdls.ogs.trieste.it). Seismic-stratigraphic analyses of the MCS and SCS profiles across the westernmost Ross Sea basins have been conducted in an IHS-Kingdom project, with analytical criteria adopting the basic principles of seismic stratigraphy. Previous studies (Brancolini et al., 1995; De Santis et al., 1995; Fielding et al., 2008; Pekar et al., 2013; Sauli et al., 2014, 2021; Pérez et al., 2021) form the framework for our broader correlations. The two main stratigraphic discontinuities of focus in this work are the ANTOSTRAT-defined Ross Sea Unconformity (RSU)5 and RSU4 (Brancolini et al., 1995). Two Ross Sea Sequences (RSS), RSS-3 and RSS-4, have previously been defined between these bounding unconformities, herein divided into four seismic units in McMurdo Sound, named RSS3-II_w, RSS3-I_w, RSS4-II_w, RSS4-I_w (upwards in stratigraphic order). These are proposed here to directly correlate to units RSS3-II, RSS3-I, RSS4-II, RSS4-I, in the central basins of the Ross Sea as defined by Pérez et al. (2021). In addition, seismic unit RSS5-II_w is identified in McMurdo Sound above RSU4 (Fig. 2). In order to maintain nomenclature consistency with the underlying sequences, its upper boundary is named RSU3a_w.

Maps of stratigraphic discontinuities, seismic sequences and units are presented in seconds two-way travel time (TWTT). They have been created by flex gridding interpolation with a 100 × 100 m cell size. The interpolation area is limited by a polygon with boundaries on the coastline, 1000 m isobath and the central axis of Crary and Mawson banks (Fig. 1). Correlations of RSU4, RSU5 and the sediment sequences between these discontinuities in the whole Ross Sea embayment are presented as supplemental material. The thickness maps of seismic units in McMurdo Sound have been simplified to highlight major depocenters (i.e., those >0.2 s TWTT) and areas of sediment absence (i.e., unit thickness = 0 s TWTT). Locally vertical measurements of some morphologies are given in meters assuming velocity of 1500 m/s. The velocity model from Sauli et al. (2021) has been used to provide depth information on those profiles in the vicinity of time-depth charts which allow depth conversion of the reflection seismic.

Core-log-seismic correlation of seismic profile ATS-05-02 and ANDRILL Site AND-2A (i.e. time-depth chart) has been based on the the velocity model created from compressional velocities (P-wave) logged on whole-core sections of the drilled site (Dunbar et al., 2009). The correlation allows characterization of the lithological and physical

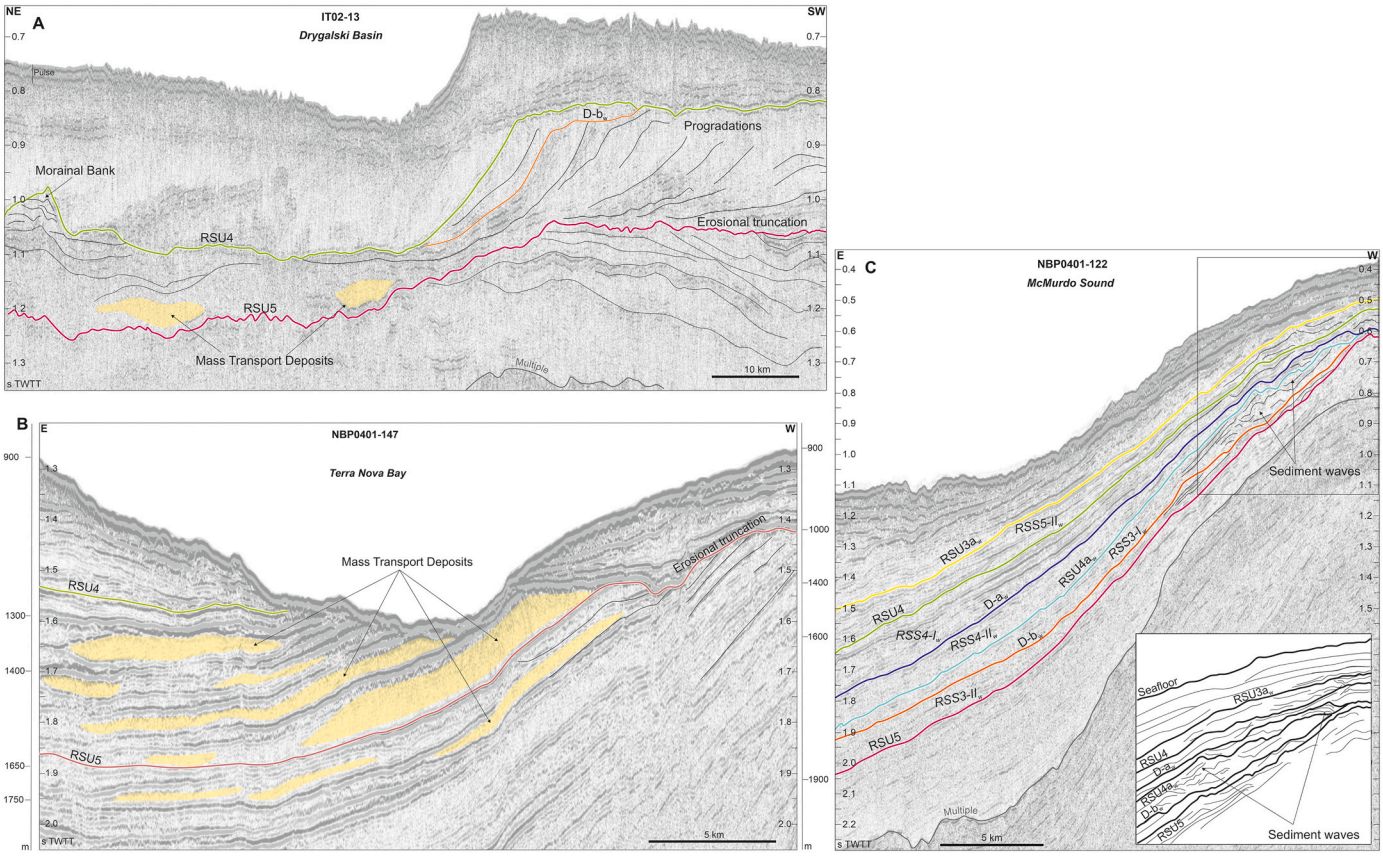

Fig. 2. Seismic line sections across the three main basins in the western Ross Sea, location in Fig. 1B. The main stratigraphic discontinuities identified in this work are named. Major sedimentary features such as erosional truncations, progradations, and mass transport deposits are highlighted according to the manuscript discussion. TWTT, two-way travel time. A) Profile IT02-13 across Drygalski Basin, note that the progradations were previously described by Sauli et al. (2014) but attributed to Pliocene glacial advance due to the previous age model. B) Profile NBP0401-147 across Terra Nova Bay. Depth in meters is included in the vertical axes based on the velocity model from (Sauli et al., 2021). C) Profile NBP0401-122 across McMurdo Sound. Detailed line-drawing of the sediment waves is included in the inset. B10

Table 1
Correlation of the stratigraphic discontinuities identified in this work with previous regional interpretations, and the proposed age ranges of stratigraphic hiatuses (including uncertainties in age model) and surfaces based on ANDRILL Site AND-2A. Mbsf, meters below seafloor.

	Depth (mbsf)	Age (Ma) as in Levy et al. (2016)	ANTOSTRAT	Fielding et al. (2008) & Pekar et al. (2013)
RSU3a$_w$	~215	(U4) ~11.08–14.4	RSU4	Rh
RSU4	~280	(U3) ~14.1–15.8	RSU4	Rg
D-a$_w$	~375	~16.2		
RSU4a$_w$	~490	~16.8	RSU4a	
D-b$_w$	~650	~17.4		
RSU5	~775	(U2) ~17.8–18.7	RSU5	Rf
D-e	~980	(U1) ~19.8–20		

properties of the defined seismic units (Supplemental material), as well providing age constraints for the interpreted stratigraphic discontinuities (Table 1). AND-2A was drilled in the inner McMurdo Sound, recovering sediments up to 1138.5 m below seafloor (mbsf) (Florindo et al., 2008). Physical properties were measured from downhole wireline tools [magnetic susceptibility, spectral gamma radiation, sonic velocity, neutron porosity and density (Wonik et al., 2009)] and core logging [wet bulk density, compressional P-wave velocity and magnetic susceptibility (Dunbar et al., 2009)]. Lithology of the described units is based on the previously published lithostratigraphy in Passchier et al. (2011) and Levy et al. (2016) where paleoenvironmental conditions were assessed by assemblages of fossil pollen, dinoflagellates, diatoms, foraminifera, and molluscs. The age constraints (Table 1) are from the updated age model by Levy et al. (2016) which built on magnetostratigraphy, biostratigraphy, $^{87}Sr/^{86}Sr$ dating of macrofossils, and $^{40}Ar—^{39}Ar$ ages on lava clasts and tephra layers.

3. Results

The seismic resolution and penetration, and the interference of the seafloor multiple limit interpretation confidence below RSU5 in most of the western Ross Sea. The imaged sedimentary record beneath RSU5 generally exhibits low amplitude reflections with variable lateral continuity. Along the westernmost margin, the reflections are tilted eastwards (Fig. 2B), and locally form mounded morphologies in McMurdo Sound. To the southeast of Coulman Island, lenticular bodies exist and are separated by high amplitude reflections (Fig. 2A).

Locally, there is angular truncation of reflections beneath RSU5, particularly at shallow depths (<1 s TWTT) in western McMurdo Sound and offshore from Terra Nova Bay (Fig. 2B, 3). Along the westernmost margin and at Mawson Bank, RSU5 is locally crosscut by overlying erosional surfaces and/or the seafloor. In McMurdo Sound, these areas of subsequent erosion extend offshore up to ~25 km from Wright Valley

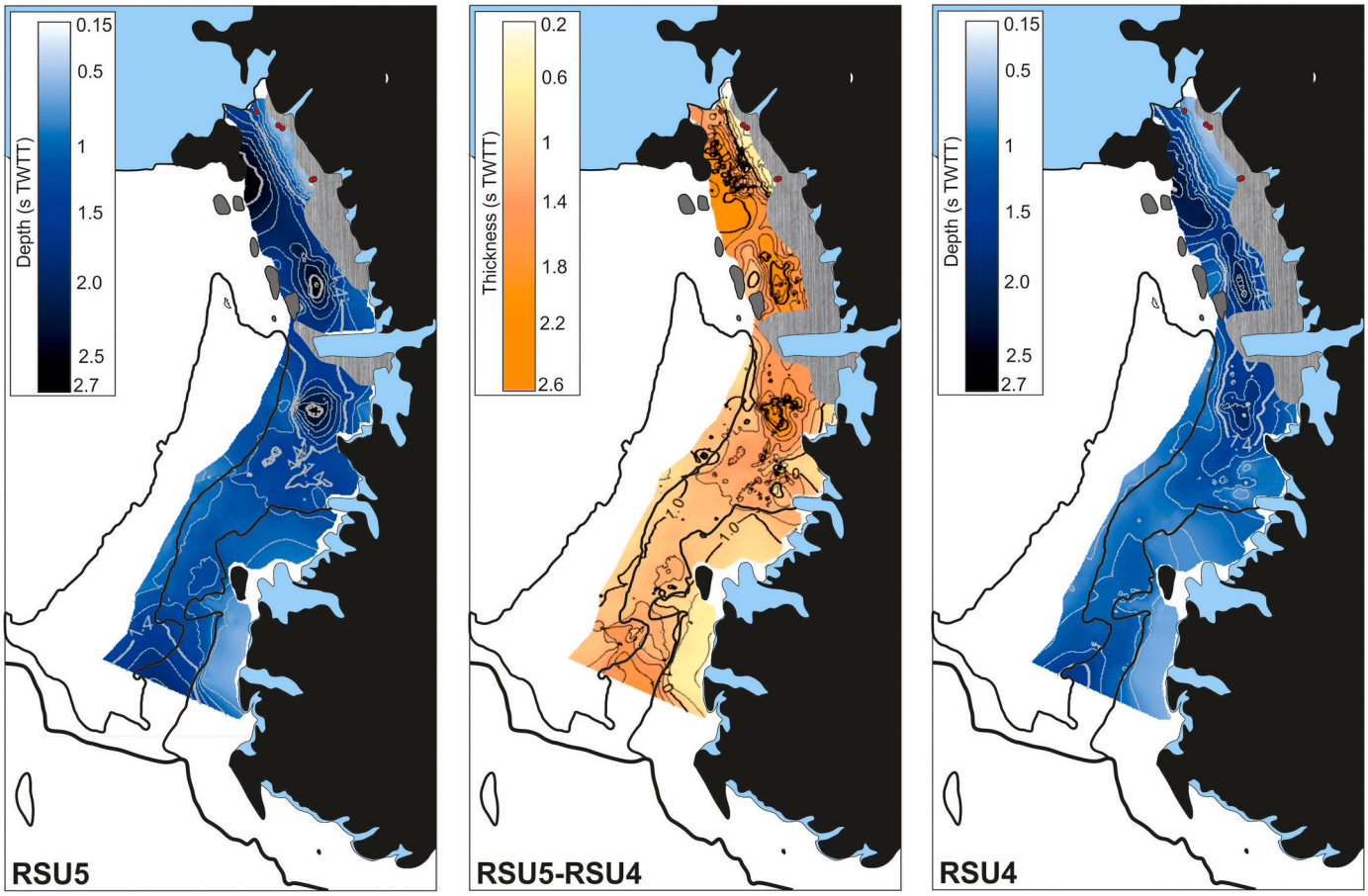

Fig. 3. Main interpreted surfaces, RSU4 and RSU5, in depth as seconds two-way travel time (TWTT) and sediment thickness between them along the western Ross Sea. Isolines at 0.2 s intervals. Modern continental shelf edge is marked by the thick black line and the thin black lines outline banks and basins. Light blue areas represent the present-day ice shelf coverage. Drilled sites in McMurdo Sound are marked with red dots.

and ~17 km from McKay Valley. The sharpest change of slope in RSU5 within McMurdo Sound is located between ~15 km (south) and 25 km (north) from the coastline (Fig. 4). In McMurdo Sound and Nordenskjöld Basin, RSU5 deepens eastwards from 0.2 to 2.5 s TWTT (Fig. 3). In the southern Drygalski Basin, RSU5 is located at 1–1.2 s TWTT depth, while in the northern part of the basin, it deepens northwards from 1.2 to >1.8 s TWTT (Fig. 3).

There is also angular truncation of reflections beneath RSU4, particularly in areas of McMurdo Sound, and along the western Drygalski Basin offshore from Coulman Island (Fig. 2A, 5A, Table 2). It is crosscut along the Mawson Bank and the coastline of Ferrar Valley (~20 km offshore), McKay Valley (~40 km offshore), and Drygalski Valley (~30 km offshore) by overlying erosional surfaces. The sharpest change in slope of the RSU4 surface is located between ~25 km (south) and ~40 km (north) from the western coastline of McMurdo Sound (Fig. 4). RSU4 deepens towards the east, from <0.4 s TWTT offshore from Scott Coast, to >2 s TWTT depths ~60 km from northern Terra Nova Bay (Fig. 2C), with the deepest depression occurring in the eastern Nordenskjöld Basin (>2.1 s TWTT) (Fig. 3).

The sedimentary record between RSU4 and RSU5 is heterogeneously distributed along the westernmost Ross Sea. It is generally thicker in McMurdo Sound and Nordenskjöld Basin (>1.5 s TWTT) than in Drygalski Basin (>0.9 s TWTT) (Fig. 3). Mound morphologies and bodies of semi-transparent seismic facies are identified between RSU5 and RSU4 in Drygalski Basin. Along the western margin, thick prograding sedimentary wedges (up to ~0.12 s TWTT thick) characterise the sedimentary record offshore from Coulman Island, below a ~0.3 s TWTT succession formed by chaotic facies interbedded with high amplitude reflections (Fig. 2A). The high resolution seismic data and core-log-seismic correlation with Site AND-2A available in McMurdo Sound enable the identification of three major stratigraphic discontinuities between RSU5 and RSU4, D-b_w (oldest), RSU4a_w and D-a_w (youngest), bounding four seismic units further described below (Fig. 2C, 6).

3.1. RSU5-RSU4 stratigraphy in McMurdo sound

3.1.1. RSS3-II_w

Above RSU5, RSS3-II_w reflections form irregular mounds offshore from the Ferrar and McKay valleys (Table 2). RSS3-II_w is absent offshore from Koettlitz Valley, and for up to ~35 km and ~15 km from the mouths of the Ferrar and Wright valleys, respectively (Fig. 7). Along the central axis of McMurdo Sound, RSS3-II_w forms a continuous cover of up to 0.20 s TWTT in the south, whereas, in the north, disconnected depocenters (>0.3 s TWTT) are elongated perpendicular to the western margin. At Site AND-2A, velocity and density decrease downwards through the unit while magnetic susceptibility is relatively homogeneous. Natural gamma radiation, porosity and water content values increase downwards (Fig. 6).

3.1.2. D-b_w and RSS3-I_w

D-b_w is crosscut by the seafloor or D-a_w ~30 km offshore from McKay Valley and ~20 km offshore from Ferrar Valley (Fig. 2, 6). The sharpest change in D-b_w slope is located 20–30 km from Scott Coast, south to north (Fig. 4, Table 2). D-b_w deepens towards the east reaching 2.6 s TWTT.

Above D-b_w, the reflections within RSS3-I_w are wavy along the western area, forming small-mounded bodies (<1 km wide) offshore from Ferrar and McKay valleys (Fig. 2C, 5B, Table 2). The major depocenter (>0.15 s TWTT) is located offshore from Koettlitz Valley, whereas the unit is absent for 17–27 km offshore from Ferrar Valley, from south

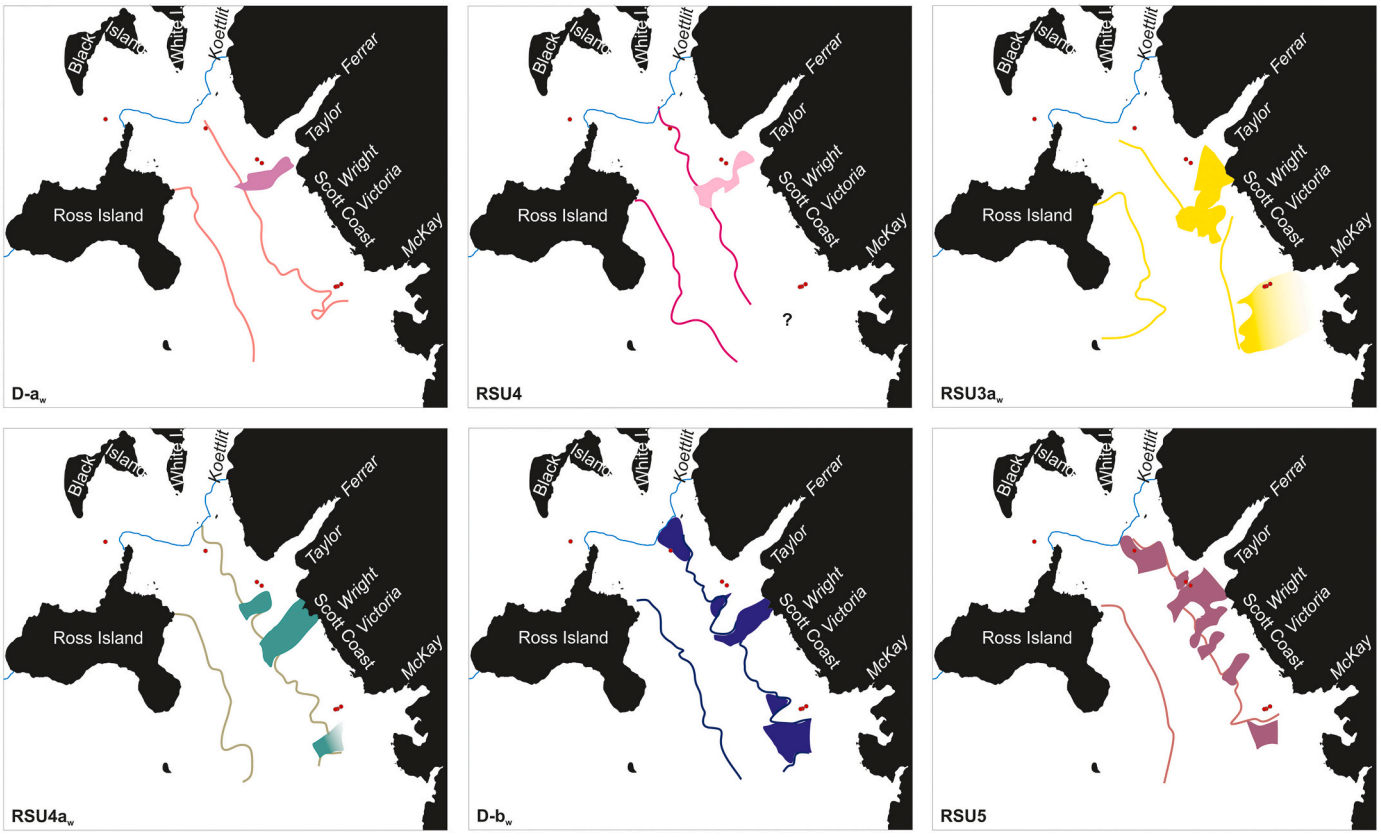

Fig. 4. Major morphological features distinguished on the interpreted stratigraphic discontinuities in McMurdo Sound. The lines represent the sharpest change of slope of the surface and the edge of the deepest depression from west (nearest to the Scott Coast) to east (nearest to Ross Island) respectively. The solid features represent location and shape of the major troughs identified on each stratigraphic discontinuity. Light blue line represents the present-day edge of the Ross Sea Ice Shelf. Drilled sites in McMurdo Sound are marked with red dots.

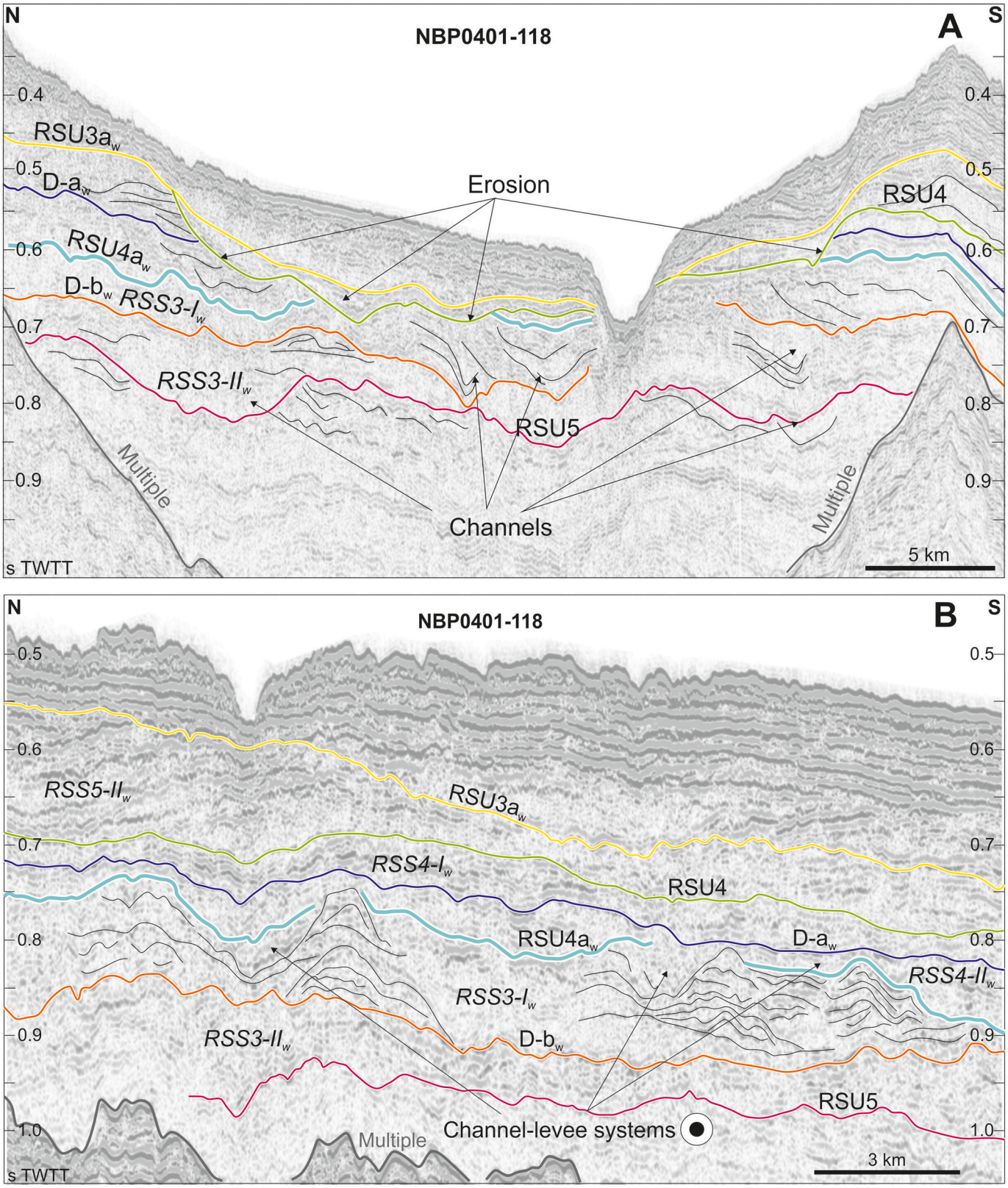

Fig. 5. Sections of seismic line NBP0401-118 along McMurdo Sound, location in Fig. 1B. The main stratigraphic discontinuities and seismic units identified in this work are named. TWTT, two-way travel time. A) Channels linked with RSU5 are indicated by arrows. Erosional truncations beneath RSU4 are also marked. B) The channel-levee systems found in unit RSS3-I$_w$ are marked.

Table 2
Main features of the stratigraphic discontinuities and seismic units distinguished in this work. Depositional features are based on ANDRILL Site AND-2A (Passchier et al., 2011; Levy et al., 2016). MCO, Miocene Climate Optimum; MMCT, Middle Miocene Climate Transition; MTD, mass transport deposit; TWTT, two-way travel time.

Sequence/ Surface	Key seismic features	Key depositional features	Interpretation	Climatic period
RSU3a$_w$	Local erosional truncation	Shift from thick (below) to thin (above) interbeds of massive diamictites Sedimentary hiatus ~1.7 myr (U4)	Glacial advance of marine-based ice and aridification of the Dry Valley regions	MMCT
RSS5-II$_w$	Local sediment waves MTDs (0.07–0.08 s TWTT)	Abundant massive diamictites	Persistent marine-based ice sheets experiencing multiple regional advances	MMCT
RSU4	Widespread angular truncation Ferrar Valley Trough (<33 m)	Shift from stratified diamictites (below) to massive diamictites (above) Sedimentary hiatus ~1.7 myr (U3) Glacial surface of erosion in AND-2A	Onset of repeated marine-based ice sheet expansion	MMCT
RSS4-I$_w$	Slightly undulating reflections Sparse sediment waves and large MTDs (~0.11 s TWTT)	Thick interbeds of stratified diamicitites sandstones and mudstones	Minimum ice sheet extent	MCO
D-a$_w$	Irregular morphology Ferrar Valley through (<17 m) Sediment Waves	Shift from thin (above) to thick (below) interbeds of stratified diamicitites sandstones and mudstones	Turbid meltwater and glacifluvial drainage from a retreated ice sheet	MCO
RSS4-II$_w$	Undulating reflections and small MTDs (<0.05 s TWTT)	Thin interbedded diamictites, sandstones and mudstones	Distal glacimarine sedimentation influenced by marine-terminating outlet glaciers and periods of major retreat of the ice sheet	MCO
RSU4a$_w$	Irregular morphology, local erosional truncation Channel systems and numerous small troughs (<6 m) offshore from the main valleys	Shift from thick (below) to thin (above) interbeds	Ice proximal environments and Short-lived ice sheet advance	MCO
RSS3-I$_w$	Limited lateral continuity Sediment waves and channel-levee systems	Thick interbeds of stratified diamictites, sandstones and mudstones	Turbiditic activity during deglaciation. Ice distal environments and relative glacial retreat	Onset of the MCO
D-b$_w$	Irregular morphology Local erosional truncation Troughs (<25 m depth x 7–9 km wide) offshore from the major fjords	Shift from interbedded massive and stratified diamictites (below) to thin interbeds of stratified diamictites, sandstones and mudstones (above)	Rapid glacimarine sedimentation from marine-terminating ice sheets Transition from subglacial/ice-proximal to ice-proximal/ice-distal conditions	Early Miocene cold
RSS3-II$_w$	Stratified reflections Localized irregular mounds	Massive and stratified diamictites Glacial shear features	Marine-terminating glacier advances Continued ice sheet expansion Ice marginal to ice distal glacimarine settings	Early Miocene cold
RSU5	Local erosional truncation Troughs (<122 m depth x 7–9 km wide) offshore form the major outlet glaciers	Shift from mudstone (below) to diamictite (above) Sedimentary hiatus ~0.9 myr (U2)	Large outlet glaciers actively downcutting Ice sheet advance	Early Miocene cold

to north respectively, and ~20 km offshore from the Taylor and Wright valleys (Fig. 7). Towards the east, RSS3-I$_w$ is >0.12 s TWTT thick, extending over a wider area in the south than in the north. At Site AND-2A, the velocity and density values generally decrease downwards in this unit. Magnetic susceptibility shows an overall trend towards lower values with increasing depth with median and mode values of 453 dimensionless [SI] and 415 [SI], respectively. The natural gamma radiation, porosity and water content tend to increase downwards in the unit (Fig. 6).

3.1.3. *RSU4a$_w$ and RSS4-II$_w$*

RSU4a$_w$ forms channel-like morphologies offshore from Ferrar, Taylor and Wright valleys (Fig. 2C, 5B, Table 2). Along the western side of McMurdo Sound, it is crosscut by RSU4 about 18 km offshore from Ferrar Valley (Fig. 5A), and by D-a$_w$ ~23 km offshore from McKay Valley (Fig. 2C, 8A). The sharpest change in slope is located 22–28 km from Scott Coast (Fig. 4). RSU4a$_w$ deepens eastwards reaching 2.7 s TWTT (Fig. 4).

RSS4-II$_w$ is absent for ~13 km offshore from Ferrar Valley, ~28 km offshore from Taylor and Wright valleys, and ~25 km offshore from McKay Valley (Fig. 7). Chaotic bodies are more abundant to the north of Scott Coast (Table 2). Along the central axis of McMurdo Sound, the thickest depocenter is located offshore from Taylor and Wright valleys reaching a maximum thickness of <0.33 s TWTT. Comparatively thinner cover is observed towards the area offshore from north of Ferrar Valley (0.12 s TWTT). Thin cover is also recorded offshore from south of McKay Valley (<0.12 s TWTT). Velocity values are highly variable through the unit in AND-2A. The magnetic susceptibility shows shifts towards lower values with 491 [SI] median and 280 [SI] mode. Natural gamma radiation show a downwards trend of increasing values (Fig. 6).

3.1.4. *D-a$_w$ and RSS4-I$_w$*

D-a$_w$ is crosscut by RSU4 along most of the southwestern McMurdo Sound. The sharpest change in slope of D-a$_w$ is located ~20–31 km from the coastline (Fig. 4). D-a$_w$ morphology is marked by a ~25 km wide band that extends ~30 km offshore from McKay Valley consisting of the top of small waves formed by undulating reflections (Fig. 2C, 8A, Table 2). The discontinuity deepens eastwards to 2.2–2.5 s TWTT.

Sparse sediment waves in RSS4-I$_w$ can be identified offshore from the Taylor, Wright, and McKay valleys where, further east, semi-transparent facies form large chaotic bodies interbedded with continuous reflections (Fig. 8, Table 2). The complete chaotic sequence is ~0.11 s TWTT thick over 775 km^2, containing approximately 77.10^6 m^3 of sediments. RSS4-I$_w$ is absent up to ~20 km offshore from Ferrar Valley, ~31 km offshore from Taylor and Wright valleys and 15–29 km offshore from McKay Valley (Fig. 7). It forms an elongated depocenter to the east of the central axis of McMurdo Sound locally reaching thickness >0.22 s TWTT. At Site AND-2A, velocity in this unit varies over a wide range of values. Density values present an overall trend of slightly downwards increase. The magnetic susceptibility shows a trend towards below-average values, with low median (318 [SI]) and mode (186 [SI]) values. The gamma radiation values decrease downwards from the top of the unit up to 346 mbsf (Fig. 6).

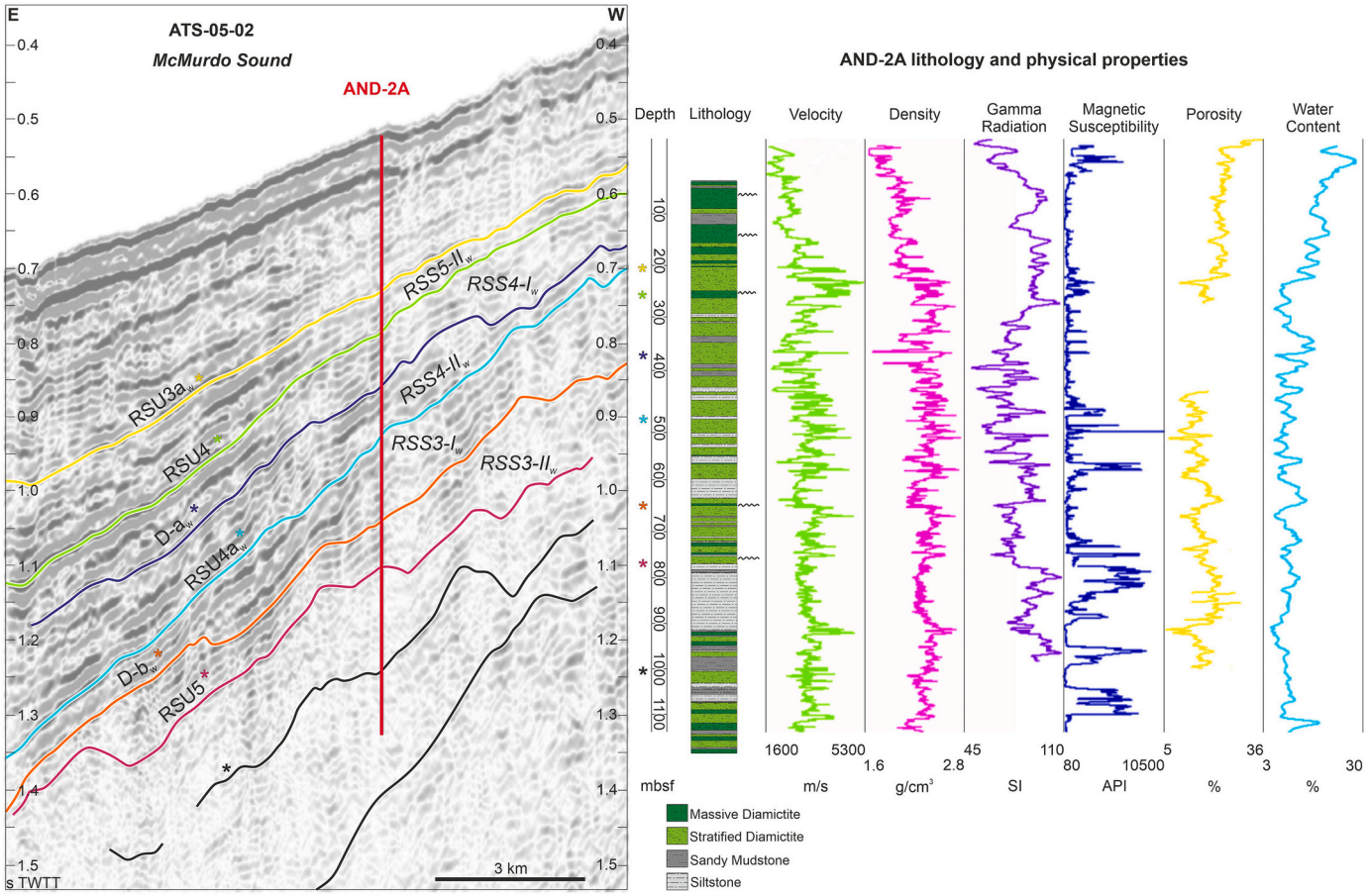

Fig. 6. Core-log-seismic correlation between seismic line ATS-05-02 and ANDRILL Site AND-2A in the southern McMurdo Sound, location in Fig. 1B. The main stratigraphic discontinuities and seismic units identified in this work are named. The location of the stratigraphic discontinuities is marked (*) in the site plots using matching colours. Lithology is simplified from Passchier et al. (2011) and Levy et al. (2016). Mbsf, meters below seafloor; TWTT, two-way travel time. The time-depth correlation is shown as supplemental material.

3.2. *RSS5-II$_w$ and RSU3a$_w$ in McMurdo sound*

Overlying RSU4, RSS5-II$_w$ internal reflections are locally wavy (Fig. 2C) and lenticular bodies of chaotic seismic facies are interbedded (Table 2). They are more prominent between the Ferrar and McKay valleys (Fig. 8B). Here, three major lenticular bodies can be distinguished. The northern body has a thickness of up to ~0.07 s TWTT over ~50 km^2 whereas the southern one is locally thicker within its ~95 km^2 area. Below the first, ~0.08 s TWTT thick body extends over ~120 km^2. The sedimentary record of RSS5-II$_w$ is very thin to absent (<0.03 s TWTT) along the western margin of McMurdo Sound (Fig. 7). The unit is not present along a fringe extending ~11 km offshore from Ferrar Valley and up to ~48 km offshore from McKay Valley. Significant thicknesses, exceeding 0.18 s TWTT, are restricted to depocenters along the eastern McMurdo Sound. A SW-NE elongated depocenter north of Ferrar Valley crosses the central axis of McMurdo Sound with maximum thickness >0.27 s TWTT (Fig. 7). At Site AND-2A, velocity values generally decrease downwards in this unit. Magnetic susceptibility values are generally low, with data displaced towards below-average values (398 [SI] median and 356 [SI] mode). The gamma radiation presents low range variability but generally shows downwards decreasing trend (Fig. 6).

At the top of RSS5-II$_w$, RSU3a$_w$ forms a regional discontinuity in McMurdo Sound (Fig. 2, 5, 8, Table 2). It is crosscut by the seafloor at ~13–17 km offshore from Ferrar Valley and ~26–28 km offshore from McKay Valley, whereas it crosscuts and truncates the underlying reflections along the western margin (Fig. 5B, 8A). The sharpest change in slope for RSU3a$_w$ is located 22–36 km offshore from Scott Coast (Fig. 4). At the mouth of the McKay and Ferrar valleys, this discontinuity truncates underlying units over ~37 km and ~15 km respectively. In the inner part of McMurdo Sound, the discontinuity presents as an irregular surface that forms an 8–5 km wide band that narrows northwards. This irregular surface is located 18–30 km offshore from the western coastline (increasingly distal to the north) with local underlying truncation terminations to the east (Fig. 5B). RSU3a$_w$ deepens to almost 2 s TWTT along the Ross Island margin.

4. Discussion

Correlations of the reflection seismic profiles in the western Ross Sea to recent seismic-stratigraphic interpretations in the central Ross Sea, integrating the age control obtained from AND-2A, IODP Expedition 374 and DSDP Leg 28 (Levy et al., 2016; Marschalek et al., 2021; Pérez et al., 2021), provide insights into the patterns of glacial advance and retreat across the Ross Sea through early to late Miocene. These correlations also enable identification of significant spatial differences in past ice sheet extent, and sediment delivery by glaciers emanating from East and West Antarctica.

Four distinct depositional units document subglacial to ice-proximal/ice-distal depositional systems in McMurdo Sound during the early to middle Miocene (RSU5 to RSU4), while paleo-channels and troughs indicate major pathways that supplied the sediment (Table 2). Local variability results from advance of coalescing lobes of marine-terminating glaciers emanating from the major EAIS outlet glaciers

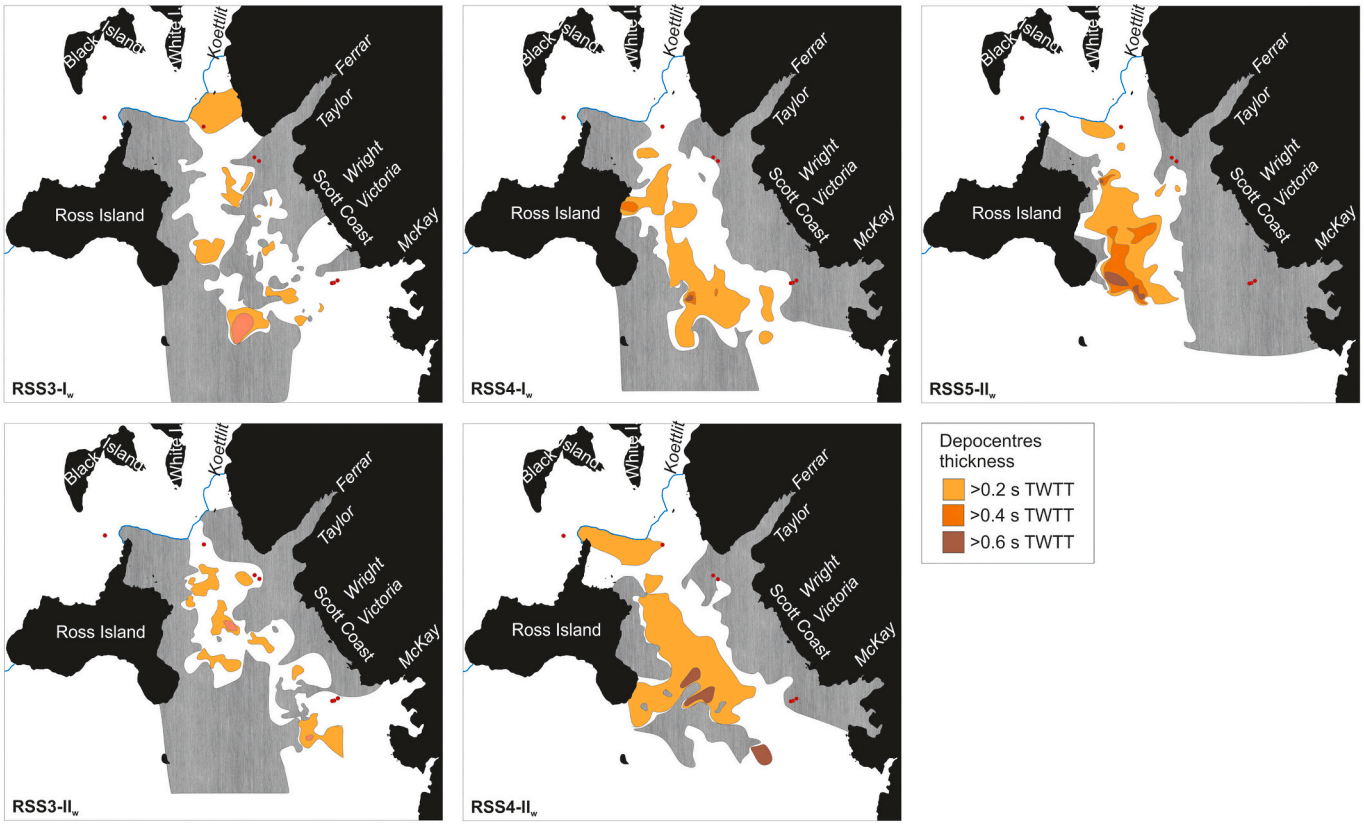

Fig. 7. Sediment distribution in the interpreted seismic units. The maps have been simplified to show the major depocentres and to highlight unit absence (0 s TWTT thickness). Light blue line represents the present-day edge of the Ross Sea Ice Shelf. Drilled sites in McMurdo Sound are marked with red dots. TWTT, two-way travel time.

that extended into deeper troughs. Offshore from Terra Nova Bay, sharp erosional truncations indicate erosion of the sedimentary record up to ~41 km from the coastline (Fig. 2B) as the result of repeated glacial overriding during the glacial cycles since the middle Miocene (Levy et al., 2016). In Drygalski Basin, localized depocenters are formed by prograding sedimentary wedges indicating ice-proximal environmental conditions, followed by ice-distal conditions recorded by a thin succession of chaotic facies (Fig. 2A, 3). The discrete bodies of chaotic facies are interpreted as mass transport deposits (MTDs) following Reading (1996). The abundance and distribution of MTDs suggests that the deep northern Drygalski Basin did not experience glacial overriding during most of the early and middle Miocene (Fig. 2A). However, sparse morainal banks are locally identified on the coastal margins (Fig. 2A). Thus, the MTDs may have been triggered by glacial erosion and sediment redistribution from glaciers and ice sheets terminating in shallower water depths. Here, we discuss how the stratigraphic architecture of the westernmost Ross Sea is interpreted to relate to major ice sheet advances of early (RSU5) and middle (RSU4) Miocene.

4.1. Early miocene: marine-based ice sheet advance into the Ross Sea

Shifts to high values of magnetic susceptibility and density around RSU5 at Site AND-2A correlate with a shift in lithostratigraphy from mudstone-rich deposits >100 m in thickness underlying RSU5 to diamictite intervals <50 m thick above it (Levy et al., 2016; Fig. 6). The facies beneath RSU5 suggest an environment influenced by a hinterland ice sheet from which glaciers fed into a coastal ice shelf along the western Ross Sea margin, alternating with periods when the glacial termini retreated inland (Table 2). Overall, these facies indicate cold and relatively stable climatic conditions (Levy et al., 2016). However, intercalated MTDs in the sedimentary record offshore from Coulman Island suggest periodic advance of coastal glacier systems in that area prior to the formation of RSU5.

RSU5 constitutes a highly erosional surface along western McMurdo Sound and offshore from Terra Nova Bay. Deep troughs are located near the mouths of the three large outlet glaciers still active today in the Koettlitz, Ferrar and McKay valleys. Smaller troughs offshore from the Taylor and Wright valleys suggest these were occupied by expanded outlet glaciers (Fig. 4, Table 2). Therefore, glacial advance along the western Ross Sea margin is linked to erosional downcutting of the Transantarctic Mountains valleys by large glaciers and glacifluvial systems prior to the MMCT, which is consistent with previous inland geomorphological studies (e.g., Sugden and Denton, 2004). The trough offshore from McKay Valley has more deeply incised flanks than the southern troughs, but in all cases ice flow occurred through eastward flow of marine-terminating EAIS outlet glaciers advancing onto the continental shelf during the early Miocene. The RSU5 surface defined here was previously identified at AND-2A as a sedimentary hiatus between ~18.7 Ma and ~17.8 Ma named U2 (Levy et al., 2016), consistent with glacial overriding. However, the erosional signature of RSU5 diminishes eastwards, with erosional truncation limited to the inner continental shelf (Pérez et al., 2021). Progradation of glacimarine strata over aggradational open-marine strata suggests that the continental shelf basins where not completely overridden by a grounded marine-based ice sheet at this time (Fig. 2A).

Above RSU5, small and local depocenters are identified in RSS3-II$_w$ along the central part of McMurdo Sound between ~17.8 Ma and ~17.4 Ma (Table 1). This unit is, however, absent offshore from the Taylor and Wright valleys probably as a result of erosion due to marine-terminating glacier advances from these fjords (Fig. 7, Table 2). The cross-shelf glacial advance triggered downslope sediment transport recorded in the irregular morphology and U-shape troughs offshore from Taylor and

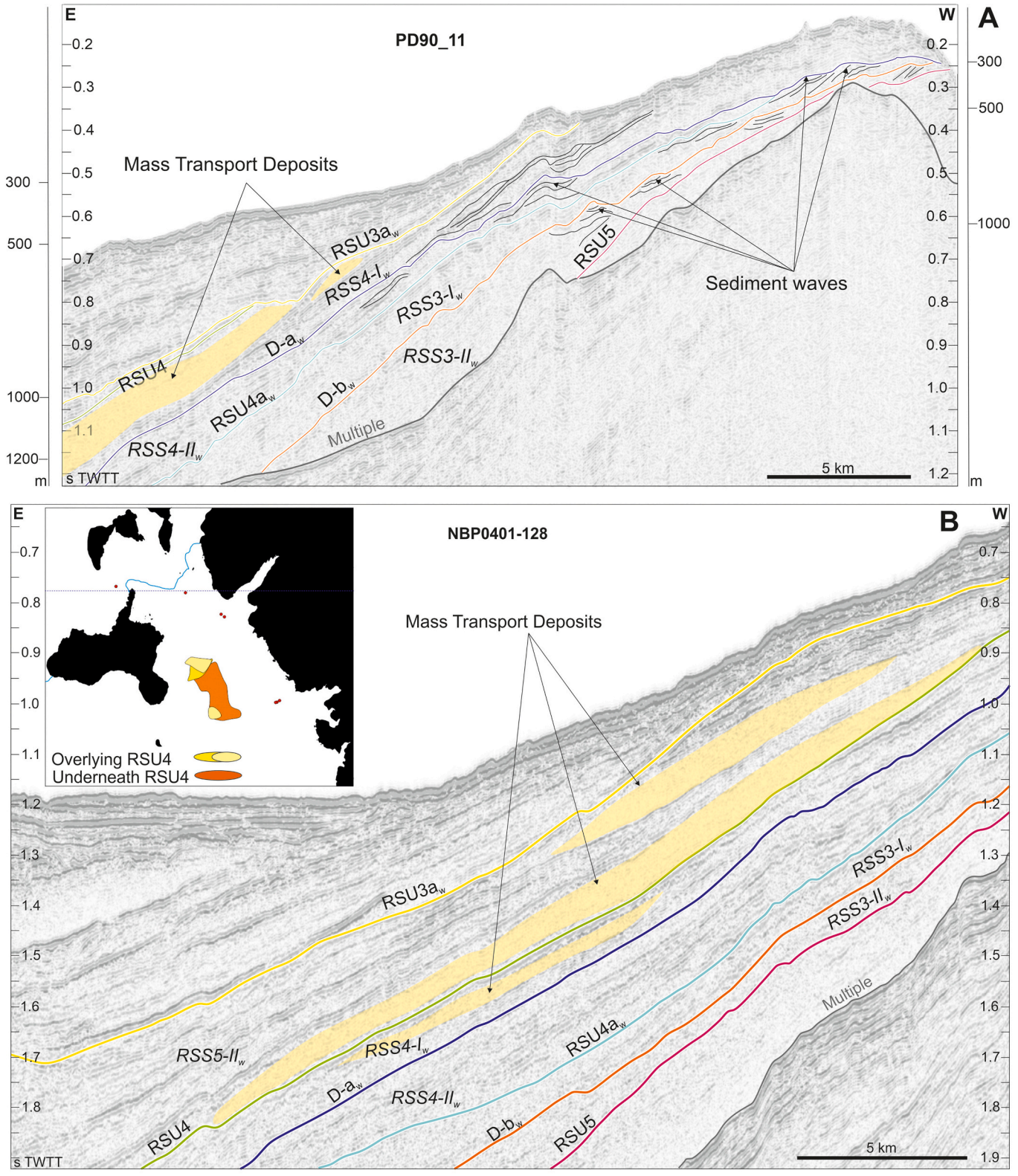

Fig. 8. Sections of seismic lines PD90-11 and NBP0401-128 in McMurdo Sound, location in Fig. 1B. The main stratigraphic discontinuities and seismic units identified in this work are named. TWTT, two-way travel time. A) Sediment waves along the western McMurdo Sound are indicated by arrows. Depth in meters is included in the vertical axes based on the velocity model from (Sauli et al., 2021). B) Large mass transport deposits are highlighted by yellow, semi-transparent fill. Their distribution in McMurdo Sound is shown in the inset with the stratigraphic position relative to RSU4 distinguished using different colour fills.

Wright valleys (Fig. 5A). Gravitational transport of reworked glaciogenic sediments is common during major ice sheet advance into the marine realm (e.g., Huang and Jokat, 2016). At Site AND-2A, RSS3-II_w is mainly formed by massive diamictites (Fig. 6), and sedimentary structures consistent with glacial shearing indicating ice sheet overriding (Passchier et al., 2011; Levy et al., 2016). Consequently, continental scale EAIS advance beyond the western Ross Sea coastline commenced ~17.8 Ma during the formation of RSU5, followed by fluctuating EAIS outlet glacier advances throughout the sedimentation of RSS3-II_w during the early Miocene (Table 1, 2).

The slow subsidence in the Terror Rift (~23–13 Ma; Fielding et al., 2008; ~23–0 Ma Sauli et al., 2021) during the formation of RSU5 and sedimentation of RSS3-II_w suggests RSU5 was a major EAIS overriding event over a shallow continental shelf coastal bench at Site AND-2A (Levy et al., 2016). At the same time, a progradational glacimarine environment at Site U1521, with a distinct provenance indicative of a large WAIS advance (Marschalek et al., 2021), points to an equally large, and highly erosive, advance in the central Ross Sea. This synchronous advance of EAIS and WAIS supports the interpretation of Marschalek et al. (2021) of a major continent-wide ice sheet advance, and cold climate between 17.8 and 17.4 Ma. The glacial advance was associated with a fall in eustatic sea-level of 40–60 m inferred from deep sea isotope records (Miller et al., 2020).

As a result of the ice sheet advance during RSS3-II_w sedimentation, the western margin of McMurdo Sound prograded ~4–6 km between RSU5 and D-b_w. Consequently, the seafloor morphology was steeper during D-b_w formation than during RSU5 (Fig. 4). Steeper slopes favor the incision of channels (Piper and Normark, 2009). Accordingly, surface D-b_w has a very irregular morphology with marked troughs offshore from the Ferrar, Victoria, and McKay valleys (Fig. 5A, Table 2). In Drygalski Basin, D-b_w forms the top of the prograding sedimentary wedges offshore Coulman Island (Fig. 2A), which have been previously described (Sauli et al., 2014). Similarly, D-b forms the top of prograding sedimentary wedges in the main basins of the central Ross Sea, interpreted as a rapid pulse of glacimarine sedimentation from marine-terminating ice sheets (Pérez et al., 2021), including ice advancing from East Antarctica (Marschalek et al., 2021). Although D-b and D-b_w cannot be continuously traced across the Ross Sea, their signature and age constraints point to continued presence of expanded marine-terminating ice sheets in the Ross Sea up to ~17.4 Ma (Fig. 6, Table 1).

4.2. Early miocene: Ice sheet retreat

Above D-b_w in McMurdo Sound, intervals with high density and low density values are interbedded within RSS3-I_w (Fig. 6), and correlate to increased deposition of mudstone-rich facies, stratified diamictites and sandstones, and general absence of massive diamictite and glacial shear structures (Passchier et al., 2011), interpreted as representing ice distal environments and relative glacial retreat (Table 2; Levy et al., 2016). Across McMurdo Sound, RSS3-I_w presents a thin cover of limited lateral continuity seismic reflections with local depocenters, thicker and more extensive than those of the underlying unit (Fig. 7). These facies suggest that the localized depocenters of RSS3-I_w resulted largely from gravity-driven processes. The largest depocenter observed is located offshore from Koettlitz Valley (Fig. 7), pointing to high flux of sediment from the southernmost fjord. Offshore from the Ferrar and Wright valleys, large troughs and absence of RSS3-I_w are probably due to active erosion resulting from advance of EAIS outlet glaciers. The RSS3-I_w reflections undulate offshore from Scott Coast, locally indicating distinct fields of sediment waves (Table 2) similar to the asymmetric buried bedforms defined by Wynn and Stow (2002). The sediment waves are spatially associated with channel-levee systems (Fig. 5B) formed by downslope turbidity flows (Longva et al., 2008). Channel-levee systems across glaciated margins are often interpreted to be associated with meltwater discharge in deglacial settings along margins previously occupied by glaciers and ice sheets (e.g., Clark and Pickering, 1996). Thus, the sediment waves and channel-levee systems in McMurdo Sound are interpreted as turbiditic in origin (Howe, 1996; Wynn and Stow, 2002). Abundant discharge of turbid subglacial meltwater during the early to middle Miocene is consistent with extensive landforms documented in Victoria Land prior to 14.8/14.4 Ma (Sugden and Denton, 2004; Lewis et al., 2006). Therefore, we interpret the facies identified in RSS3-I_w as recording widespread turbiditic activity that occurred during deglaciation following a period of marine ice sheet advance. The variability in the depositional patterns from the seismic and lithological data between RSS3-II_w and RSS3-I_w (Fig. 5) suggests a transition from subglacial/ice-proximal to ice-proximal/ice-distal conditions migrating southwards in McMurdo Sound (Table 2), and may correlate with a trend towards 40–60 m higher eustatic sea level between 17.4 and 16.8 Ma as inferred from deep-sea benthic foraminiferal oxygen isotopes and Mg/Ca records, albeit with high-frequency, orbitally-paced variations of ~20–30 m (Miller et al., 2020).

4.3. Middle miocene: Short-term ice sheet advance

RSU4a_w presents irregular morphology along McMurdo Sound, constituting a strong erosional surface offshore from McKay Valley (Table 2). Troughs offshore from the Ferrar, Taylor, Wright and McKay valleys have narrower morphologies with respect the underlying discontinuity (D-b_w) but maintain the same orientation (Fig. 4). Thus, the glacial advances followed the same pathways at ~16.8 Ma as the previous glacial peak (~17.4 Ma). Numerous channels to the south of Ferrar Valley (Fig. 5B) are consistent with widespread erosion by turbidity currents initiated as a result of high volumes of turbid meltwater discharge during nucleation of the ice sheet (e.g., Greenwood et al., 2007). These meltwater rich glacial systems are also characterized by large volumes of sediments reworked by gravitational flows often associated with ice sheet advance (Solli et al., 2007; Huang and Jokat, 2016). Thus, the RSU4a_w morphology is consistent with episodic ice sheet advance along Scott Coast matching the ice proximal environments in Site AND-2A (Levy et al., 2016). However, this event was not highly erosional in offshore settings since the unconformity is locally identified, and massive diamictite and glacial shear features are lacking in AND-2A at this level (Passchier et al., 2011).

Equivalent localized ice growth on isolated ice caps nucleating on bathymetric highs has been identified across the central Ross Sea basins during a similar time period (RSU4a surface in De Santis et al., 1995; Pérez et al., 2021). Therefore, localized ice growth may have occurred regionally across the Ross Sea during a short-term interval linked with a low amplitude sea level fall after the onset of the MCO at 17.0 Ma (Levy et al., 2016; Miller et al., 2020).

4.4. Miocene climate optimum: Minima of ice extent and extensive glacial meltwater drainage

Surface D-a_w is dated at ~16.2 Ma in AND-2A (Fig. 6, Table 1, 2). The sedimentary record of RSS4-II_w is localized on the eastern side of McMurdo Sound and interpreted as a result of downslope sediment transport (Fig. 7). Lithostratigraphy throughout the deposition of this unit indicates cycles of distal glacimarine sedimentation influenced by marine-terminating glaciers and periods of major retreat of the EAIS, when extensive tundra occupied the coastal regions (Passchier et al., 2011; Levy et al., 2016). Sedimentation rates in glacial systems affected by surface melting are considerably higher than for colder glacial regimes where oceanic melt and iceberg calving dominate (McKay et al., 2009). Interpretation of a large sediment supply during this period is also supported by a large MTD offshore from the Wright Valley suggesting this valley, which is now arid and deglaciated, was a major conduit for the release of sediments into the McMurdo Sound during the MCO (Fig. 8).

Progradation of ~9 km occurred between RSU4a_w and D-a_w. The troughs identified on D-a_w are narrower and of limited extent, compared

to the equivalents of RSU4a$_w$ (Fig. 4). D-a$_w$ morphology is formed by small sediment waves along western McMurdo Sound (Fig. 2C, 8A, Table 2), which are consistent with widespread downslope transport fed by turbid meltwater and glacifluvial drainage from a retreated ice sheet on which there is extensive surface melting (Longva et al., 2008). Retreat of marine-terminating glaciers, alongside enhanced surface meltwater drainage is also consistent with pollen and isotopic tracers from leaf-wax biomarkers that indicate precipitation was greatly enhanced at this time, coinciding with a period of peak warmth within the early phase of the MCO (Feakins et al., 2012; Levy et al., 2016; Sangiorgi et al., 2018).

Overlying surface D-a$_w$, Unit RSS4-I$_w$ presents lithofacies alternations similar to those of the underlying unit in AND-2A (Table 2), but thicker interbeds of stratified diamicitite and sandstone/mudstone together with sedimentary proxies suggest the warmest environments in AND-2A record. In addition, a thin diatom-rich interval is preserved and interpreted as representing maximum ice sheet retreat (Feakins et al., 2012; Levy et al., 2016). Thus, the reduced ice sheet extent alongside enhanced surface meltwater drainage continued during the deposition of this unit. The age of RSS4-I$_w$ in AND-2A is ~16.3–15.8 Ma, but its upper boundary is a major erosional truncation that has eroded the record between 15.8 and 14.1 Ma (Fig. 6, Table 2). Consequently, although the record is not preserved, these warm and wet conditions potentially persisted until 14.1 Ma, which coincides with the onset of cooling that led to the termination of the MCO, as interpreted from deep-sea benthic foraminiferal $\delta^{18}O$ (Holbourn et al., 2014).

4.5. Middle miocene climatic transition: Extensive marine-based ice sheet advance and development of the McMurdo dry valleys

In McMurdo Sound, RSU4 constitutes an erosional surface including deep troughs carved off the Ferrar and Taylor valleys (Fig. 4, Table 2). A sharp slope change, relative to the underlying discontinuity (D-a$_w$) is interpreted as the result of ice sheet progradation from the EAIS onto the shallow coastal margin. As noted above, RSU4 is a major erosional event in AND-2A, with a 1.8 Myr-long hiatus (Table 1, 2), related to maximum ice sheet advance along the western McMurdo Sound (Levy et al., 2016). The shift in lithofacies and abundant shear fabrics above this surface (<14.1 Ma) are interpreted as representing the onset of grounded marine-based ice sheet expansion over the site (Passchier et al., 2011).

The marine-based ice sheet advance associated with RSU4 is recorded along most of the western Ross Sea margin. In the western margin of Drygalski Basin, it constitutes a strong erosional truncation of underlying progradational strata (Fig. 2A). Within Nordenskjöld Basin, RSU4 correlates to the local Rg horizon, which was interpreted in Fielding et al. (2008) and Pekar et al. (2013) in Victoria Land Basin, while the RSU4 unconformity is identified widely across the Ross Sea by its erosional signature (Brancolini et al., 1995; Pérez et al., 2021). Overall, the broad formation of RSU4 and drill site age controls indicate that it is related to widespread marine-based ice sheet advance across the Ross Sea, with associated shifting of sedimentary depocenters during the onset of the MMCT (Levy et al., 2016; Pérez et al., 2021).

Above RSU4, RSS5-II$_w$ is formed by massive diamictite facies assemblages suggestive of more persistent marine-based ice sheets associated with the RSU4 erosive surface (Passchier et al., 2011; Fig. 6, Table 1, 2). In other polar regions, large MTDs (Fig. 8B) commonly represent glacially-influenced debris flows (Pickering and Hiscot, 2016). The occurrence of MTDs intercalated with stratified reflections suggests multiple point sources of gravity flow over time (Solli et al., 2007), implying multiple regional ice sheet advances in McMurdo Sound.

The upper boundary of RSS5-II$_w$ in AND-2A (U4) formed sometime after ~14.4 Ma, and is mapped as RSU3a$_w$. Although constraining a minimum age for RSU3a$_w$ is difficult, the overlying strata are younger than ~13.8 Ma and possibly <11.08 Ma (Levy et al., 2016). RSU3a$_w$ is a highly erosional surface along the western margin of McMurdo Sound (Table 2). The truncation reaches further offshore from McKay Valley with respect to the southern glaciers, while the trough formed off Ferrar Valley is wider and offset to the north relative to the underlying discontinuities (Fig. 4). These observations suggest glacial advance of marine-based ice in the McMurdo region was derived from EAIS outlet glaciers focused on the Ferrar and McKay valleys following the MMCT, at the expense of the smaller and more even discharge from glacial and glacifluvial systems out of the Dry valleys prior to that time. This is consistent with inland evidence of aridification, reduced erosion, and downcutting of the Dry valleys (Sugden and Denton, 2004; Lewis et al., 2006; Levy et al., 2022).

The large cooling step that occurred during the MMCT is proposed to have passed the threshold that allowed perennial sea ice on high latitude margins (Levy et al., 2016). It is likely these feedbacks led to enhanced, and prolonged cold conditions resulting on several steps of regional ice sheet advance which eroded most of the sedimentary record along the inner continental shelf and western Ross Sea margin, forming the truncated, and closely spaced erosional surfaces of RSU4 and RSU3a$_w$. Ice sheet advances that follow the MMCT are characterized by large marine-based extents forming widespread erosional surfaces across the Ross Sea (e.g., Kim et al., 2018) and deposition of numerous grounding zone wedges in middle to outer shelf settings (e.g., Bart, 2003). The presence of grounding zone wedges, which form at the grounded to floating margin of marine-based ice sheets (Dowdeswell et al., 2016) within the RSS5-II$_w$ unit, help to confirm the sedimentological interpretations of cold, polar style marine-based ice sheet at AND-2A (Passchier et al., 2011; Levy et al., 2016) and the base of AND-1B (McKay et al., 2009). However, these cores only recovered small snapshots of time (~0.2 Myrs). The late Miocene record of proximal glacimarine sedimentation is poorly documented, providing few clues about the dynamics of the Antarctic ice sheets at this time (McKay et al., 2009; Wilson et al., 2012). Recovering such a record could be achieved by drilling in the deep water basin depocenters in the eastern reaches of McMurdo sound, as well as in the northern and eastern basins of the Ross Sea (Pérez et al., 2021).

5. Conclusions

The core-log-seismic correlation of high resolution seismic profiles and physical properties logged at the ANDRILL Site AND-2A enables regional interpretation of major changes in ice sheet dynamics that occurred in McMurdo Sound during the early and middle Miocene. Further comparison of the seismic facies with those identified in profiles available towards the northwest i.e., in the Nordenskjöld and Drygalski Basins, allows comparison of the major sedimentary changes across the westernmost Ross Sea with those previously identified in the central Ross Sea during the MCO and the MMCT.

Distinct formation of turbiditic channels, mass transport deposits and sediment waves suggest regional variability in glacial/deglacial processes across the westernmost Ross Sea. Carving of troughs across the Transantarctic Mountains margin during the early Miocene, together with deposition of prograding sedimentary wedges in the deepest environments, suggests large volumes of sediment were discharged from marine-terminating glaciers or glacifluvial systems at the time of RSU5 formation (~18–17.8 Ma). A period of ice sheet advance interpreted in sedimentary facies from AND-2A is represented by irregular morphologies and troughs beneath D-b$_w$ (~17.4 Ma). Widespread formation of turbiditic channel-levee systems along the western margin of McMurdo Sound and mass transport deposits in Drygalski Basin indicate subsequent ice sheet retreat during the MCO with extensive discharge of turbid meltwater. Open-marine to ice-distal conditions dominated between 17.4 Ma and 15.8 Ma, but they were interrupted by a short-lived ice sheet advance over the continental shelf at ~16.8 Ma, locally forming RSU4a$_w$/RSU4a.

Deglaciation during the MCO was followed by major marine-based ice sheet advances after ~14.1 Ma. Shelf-wide erosional events are linked to the formation of RSU4 and RSU3a$_w$, marking the expansion of

EAIS and WAIS during the MMCT. Intermittent sediment records indicating subglacial/ice-proximal conditions have been recovered after 14.1 Ma, with numerous marine-based ice sheet advances resulting in short stratigraphic snapshots at AND-2A and U1521. The presence of glacigenic debris flows in the sedimentary record of the westernmost Ross Sea, alongside earlier studies of inland geomorphology and stratigraphy, suggest regular ice sheet extension to the shelf edge and a fundamental shift in the sediment pathways with deposition of glacially eroded detritus derived from the Transantarctic Mountains. After the MMCT, the EAIS shifted into a colder glacial regime, changing the Transantarctic Mountains outlet glacier flow and leading to the aridification and development of the Dry Valleys since that time.

Supplementary data to this article can be found online at https://doi.org/10.1016/j.gloplacha.2022.103891.

Declaration of Competing Interest

The authors declare that they have no known competing financial interests or personal relationships that could have appeared to influence the work reported in this paper.

Acknowledgements

This work has received funding from the European Union's Horizon 2020 research and innovation program under the Marie Sklodowska-Curie grant agreement number 792773: West Antarctic Margin Signatures of Ice Sheet Evolution. This project contributes to the British Antarctic Survey (BAS) Polar Science for Planet Earth Programme, which also funded RDL. Most of the multichannel seismic profiles used in this work are available at the Antarctic Seismic Data Library System (https://sdls.ogs.trieste.it) under the auspices of the Scientific Committee on Antarctic Research (SCAR) policy. We acknowledge the scientific contribution from Stuart Henrys (GNS science) and Terry Wilson (The Ohio State University) towards the realization of this work. RMM funding was provided by the Royal Society Te Apārangi Marsden Fund (18-VUW-089). RMM, TRN and RHL were funded by New Zealand Ministry of Business, Innovation and Employment through the Antarctic Science Platform (ANTA1801). LD funding was provided by the Italian National Antarctic Research Program (PNRA 16_00016 and 19_00022 projects). We are grateful to N. Wardell from the National Institute of Oceanography and Applied Geophysics (OGS), for his help with the seismic database. The IHS-Kingdom project was supported through academic licenses released to BAS and OGS. This research is a contribution to the SCAR program Instabilities and Thresholds in Antarctica: The Antarctic contribution to global sea-level (INSTANT). We acknowledge the review the two anonymous reviewers which greatly improved the initial version of this work.

References

Anderson, J.B., Simkins, L.M., Bart, P.J., De Santis, L., Halberstadt, A.R.W., Olivo, E., Greenwood, S.L., 2019. Seismic and geomorphic records of Antarctic Ice Sheet evolution in the Ross Sea and controlling factors in its behaviour. v. 475, no. 1, pp. 223–240.

Arndt, J.E., Werner, S.H., Martin, J.O.N.F., Gwen, B., Bruce, G., Michele, R., Fernando, B., Jongkuk, H., Jenny, B., Rudolf, G., Gleb, U., Felipe, B., Walter, R.-P., Morishita, T., Rochelle, W., 2013. The International Bathymetric Chart of the Southern Ocean (IBCSO) Version 1.0—a new bathymetric compilation covering circum-Antarctic waters. Geophys. Res. Lett. 40, 3111–3117.

Barrett, P.J., 1989. Introduction, in Antarctic Cenozoic history from the CIROS-1 Drillhole, McMurdo Sound, Antarctica, pp. 5–6. In: Barrett, P.J. (Ed.), Department of Scientific and Industrial Research Bulletin. DSIR Publishing, Wellington, p. 245.

Bart, P.J., 2003. Were West Antarctic Ice Sheet grounding events in the Ross Sea a consequence of East Antarctic Ice Sheet expansion during the middle Miocene? Earth Planet. Sci. Lett. 216 (1–2), 93–107.

Bart, P., De Santis, L., 2012. Glacial Intensification during the Neogene: a Review of Seismic Stratigraphic evidence from the Ross Sea, Antarctica, Continental Shelf. Oceanography 25 (3), 166–183.

Brancolini, G., Busetti, M., Coren, F., De Cillia, C., Marchetti, M., De Santis, L., Zanolla, C., Cooper, A.K., Cochrane, G.R., Zayatz, I., Belyaev, V., Knyazev, M., Vinnikovskaya, O., Davey, F.J., Hinz, K., 1995. ANTOSTRAT Project, seismic stratigraphic atlas of the Ross Sea, Antarctica. In: Cooper, A.K., Barker, P.F., Brancolini, G. (Eds.), Geology and Seismic Stratigraphy of the Antarctic Margin. Antarctic Research Series, 68. AGU Washington D.C., 22 plates.

Cande, S.C., Stock, J.M., Müller, R.D., Ishihara, T., 2000. Cenozoic motion between East and West Antarctica. Nature 404, 145–150.

Clark, J.D., Pickering, K.T., 1996. Submarine Channels: Processes and Architecture. Vallis Press, London.

Davey, F.J., Brancolini, G., 1995. The late Mesozoic and Cenozoic structural setting of the Ross Sea region: Antarct. Res. Ser. 68, 167–182.

De Santis, L., Anderson, J.B., Brancolini, G., Zayatz, I., 1995. Seismic Record of late Oligocene through Miocene Glaciation on the Central and Eastern Continental Shelf of the Ross Sea. Geol. Seismic Stratigrap. Antarctic Margin 68, 235–260.

Dowdeswell, J.A., Canals, M., Jakobsson, M., Todd, B.J., Dowdeswell, E.K., Hogan, K.A., 2016. Atlas of Submarine Glacial Landforms: Modern, Quaternary and Ancient in Society, 46. Geological Society, London.

Dunbar, G. B., Atkins, C., Magens, D., Niessen, F., And the ANDRILL Scientific Team, 2009, Physical properties of sediment core AND-2A core, ANDRILL Southern McMurdo Sound Project, Antarctica. Terra Antartica, 15(1), 49-56, hdl:10013/epic.35202.d001, PANGAEA.

Eagles, G., Gohl, K., Larter, R.D., 2004. High-resolution animated tectonic reconstruction of the South Pacific and West Antarctic Margin. Geochem. Geophys. Geosyst. 5.

Feakins, S., Warny, S., Lee, J.E., 2012. Hydrologic cycling over Antarctica during the Middle Miocene warming. Nat. Geosci. 5, 557–560. https://doi.org/10.1038/ngeo1498.

Fielding, C.R., Thomson, M.R.A., 1999. Studies from the Cape Roberts Project, Ross Sea Antarctica, initial Report on CRP-2/2A. Terra Antartica 6 (1/2), 173 pp, hdl:10013/epic.28290.d001, PANGAEA.

Fielding, C., Atkins, C., B, K.N., B, G.H., Dunbar, G., Field, B., Frank, T., Krissek, L., Panter, K., Passchier, S., Pekar, S., Sandroni, S., Talarico, F., the ANDRILL Scientific Team, 2008. Sedimentology and stratigraphy of the AND-2A core, ANDRILL Southern McMurdo Sound Project, Antarctica. Terra Antartica 15, 77–112.

Florindo, F., Harwood, D., Levy, R., the ANDRILL Scientific Team, 2008. ANDRILL's Success during the 4th International Polar Year. Sci. Drill. 6, 29–31.

Granot, R., Dyment, J., 2018. Late Cenozoic unification of East and West Antarctica. Nat. Commun. 9, 3189.

Greenwood, S.L., Clark, C.D., Hughes, A.L., 2007. Formalising an inversion methodology for reconstructing ice-sheet retreat patterns from meltwater channels: application to the British Ice Sheet. J. Quatern. Scie.: Publis. Quatern. Res. Assoc. 22 (6), 637–645.

Holbourn, A., Kuhnt, W., Lyle, M., Schneider, L., Romero, O., Andersen, N., 2014. Middle Miocene climate cooling linked to intensification of eastern equatorial Pacific upwelling. Geology 42, 19–22.

Howe, J.A., 1996. Turbidite and contourite sediment waves in the northern Rockall Trough, North Atlantic Ocean. Sedimentology 43 (2), 219–234. https://doi.org/10.1046/j.1365-3091.1996.d01-1.x.

Huang, X., Jokat, W., 2016. Middle Miocene to present sediment transport and deposits in the Southeastern Weddell Sea, Antarctica. Glob. Planet. Chang. v. 139, 211–225.

Kim, S., De Santis, L., Hong, J.K., Cottlerle, D., Petronio, L., Colizza, E., Kim, Y.-G., Kang, S.-G., Kim, H.J., Kim, S., Wardell, N., Geletti, R., Bergamasco, A., McKay, R., Jin, Y.K., Kang, S.-H., 2018. Seismic stratigraphy of the Central Basin in northwestern Ross Sea slope and rise, Antarctica: Clues to the late Cenozoic ice-sheet dynamics and bottom-current activity. Mar. Geol. 395, 363–379.

Levy, R., Harwood, D., Florindo, F., Sangiorgi, F., Tripati, R., Von Eynatten, H., Gasson, E., Kuhn, G., Tripati, A., DeConto, R., Fielding, C., Field, B., Golledge, N., McKay, R., Naish, T., Olney, M., Pollard, D., Schouten, S., Talarico, F., Warny, S., Willmott, V., Acton, G., Panter, K., Paulsen, T., Taviani, M., 2016. Antarctic ice sheet sensitivity to atmospheric CO2 variations in the early to mid-Miocene. Proc. Natl. Acad. Sci. U. S. A. 113 (13), 3453–3458.

Levy, R.H., Dolan, A.M., Escutia, C., Gasson, E.G.W., McKay, R.M., Naish, T., Patterson, M.O., Pérez, L.F., Shevenell, A.E., Flierdt, T.v.d., Dickinson, W., Kowalewski, D.E., Meyers, S.R., Ohneiser, C., Sangiorgi, F., Williams, T., Chorley, H. K., Santis, L.D., Florindo, F., Golledge, N.R., Grant, G.R., Halberstadt, A.R.W., Harwood, D.M., Lewis, A.R., Powell, R., Verret, M., 2022. Chapter 9 - Antarctic environmental change and ice sheet evolution through the Miocene to Pliocene – A perspective from the Ross Sea and George V to Wilkes Land Coasts. In: Florindo, F., Siegert, M., Santis, L.D., Naish, T. (Eds.), Antarctic Climate Evolution, Second edition. Elsevier, Amsterdam, pp. 389–521.

Lewis, A.R., Marchant, D.R., Kowalewski, D.E., Baldwin, S.L., Webb, L.E., 2006. The age and origin of the Labyrinth, western Dry Valleys, Antarctica: evidence for extensive middle Miocene subglacial floods and freshwater discharge to the Southern Ocean. Geology 34.

Longva, O., Olsen, H.A., Piper, D.J.W., Rise, L., Thorsnes, T., 2008. Late glacial fans in the eastern Skagerrak; depositional environment interpreted from swath bathymetry and seismostratigraphy. Mar. Geol. 251 (1–2), 110–123.

Marschalek, J.W., Zurli, L., Talarico, F., van de Flierdt, T., Vermeesch, P., Carter, A., Beny, F., Bout-Roumazeilles, V., Sangiorgi, F., Hemming, S.R., Pérez, L.F., Colleoni, F., Prebble, J.G., van Peer, T.E., Perotti, M., Shevenell, A.E., Browne, I., Kulhanek, D.K., Levy, R., Harwood, D., Sullivan, N.B., Meyers, S.R., Griffith, E.M., Hillenbrand, C.D., Gasson, E., Siegert, M.J., Keisling, B., Licht, K.J., Kuhn, G., Dodd, J.P., Boshuis, C., De Santis, L., McKay, R.M., IODP Expedition 374 Scientists, 2021. A large West Antarctic Ice Sheet explains early Neogene Sea-level amplitude. Nature 600, 450–455.

McKay, R., Browne, G., Carter, L., Cowan, E., Dunbar, G., Krissek, L., Naish, T., Powell, R., Reed, J., Talarico, F., Wilch, T., 2009. The stratigraphic signature of the late Cenozoic Antarctic Ice Sheets in the Ross Embayment. GSA Bull. 121, 1537–1561.

McKay, R., De Santis, L., Kulhanek, D.K., IODP Expedition 374 Scientists, 2019. Ross Sea West Antarctic Ice Sheet History. International Ocean Discovery Program, Proceedings of the International Ocean Discovery Program, Colleague Station, Texas.

McKay, R.M., Escutia, C., De Santis, L., Donda, F., Duncan, B., Gohl, K., Gulick, S., Hernández-Molina, J., Hillenbrand, C.-D., Hochmuth, K., Kim, S., Kuhn, G., Larter, R., Leitchenkov, G., Levy, H., Naish, R.R., O'Brien, T., Pérez, P.F., Shevenell, A.L.E., Williams, T., 2022. Chapter 3 - Cenozoic history of Antarctic glaciation and climate from onshore and offshore studies. In: Florindo, F., Siegert, M., Santis, L.D., Naish, T. (Eds.), Antarctic Climate Evolution, Second edition. Elsevier, Amsterdam, pp. 41–164.

Miller, K.G., Browning, J.V., Schmelz, W.J., Kopp, R.E., Mountain, G.S., Wright, J.D., 2020. Cenozoic Sea-level and cryospheric evolution from deep-sea geochemical and continental margin records. Science. Advances 6, eaaz1346.

Naish, T.R., Woolfe, K.J., Barrett, P.J., Wilson, G.S., Atkins, C., Bohaty, S.M., Bucker, C. J., Claps, M., Davey, F.J., Dunbar, G.B., Dunn, A.G., Fielding, C.R., Florindo, F., Hannah, M.J., Harwood, D.M., Henrys, S.A., Krissek, L.A., Lavelle, M., van der Meer, J., McIntosh, W.C., Niessen, F., Passchier, S., Powell, R.D., Roberts, A.P., Sagnotti, L., Scherer, R.P., Strong, C.P., Talarico, F., Verosub, K.L., Villa, G., Watkins, D.K., Webb, P.-N., Wonik, T., 2001. Orbitally induced oscillations in the East Antarctic ice sheet at the Oligocene/Miocene boundary. Nature 413 (6857), 719–723.

Naish, T., Powell, R.D., Levy, R., 2007. Studies from the ANDRILL, McMurdo Ice Shelf Project, Antarctica. Initial Science Report on AND-1B. Terra Antarct. 14, no. 3.

Passchier, S., Browne, G., Field, B., Fielding, C.R., Krissek, L.A., Panter, K., Pekar, S.F., 2011. Early and middle miocene antarctic glacial history from the sedimentary facies distribution in the AND-2A drill hole Ross sea, Antarctica. Bull. Geol. Soc. Am. 123 (11–12), 2352–2365.

Paxman, G.J.G., Jamieson, S.S.R., Hochmuth, K., Gohl, K., Bentley, M.J., Leitchenkov, G., Ferraccioli, F., 2019. Reconstructions of Antarctic topography since the Eocene–Oligocene boundary. Palaeogeogr. Palaeoclimatol. Palaeoecol. 535.

Pekar, S., Speece, M., Wilson, G., Sunwall, D., Tinto, K., 2013. The Offshore New Harbour Project: Deciphering the Middle Miocene through Late Eocene Seismic Stratigraphy of Offshore New Harbour, Western Ross Sea, vol. v. 381. Geological Society of London Special Publications, Antarctica, pp. 199–213.

Pérez, L.F., De Santis, L., McKay, R.M., Larter, R.D., Ash, J., Bart, P.J., Böhm, G., Brancatelli, G., Browne, I., Colleoni, F., Dodd, J.P., Geletti, R., Harwood, D.M., Kuhn, G., Sverre Laberg, J., Leckie, R.M., Levy, R.H., Marschalek, J., Mateo, Z., Naish, T.R., Sangiorgi, F., Shevenell, A.E., Sorlien, C.C., van de Flierdt, T., IODP Expedition 374 Scientists, 2021. Early and middle Miocene ice sheet dynamics in the Ross Sea: results from integrated core-log-seismic interpretation. GSA Bull. https://doi.org/10.1130/B35814.1.

Pickering, K.T., Hiscot, R.N., 2016. In: Wiley, A. (Ed.), Deep Marine Systems. Processes, deposits, Environments, Tectonics and Sedimentation. AGU & Wiley, Oxford, p. 657.

Piper, D., Normark, W., 2009. Processes that Initiate Turbidity Currents and their Influence on Turbidites: a Marine Geology Perspective. J. Sediment. Res. - J SEDIMENT RES 79, 347–362.

Reading, H.G., 1996. Sedimentary environments. In: Processes, Facies and Stratigraphy. Blackwell Science, p. 688.

Sangiorgi, F., Bijl, P.K., Passchier, S., Salzmann, U., Schouten, S., McKay, R., Cody, R.D., Pross, J., van de Flierdt, T., Bohaty, S.M., Levy, R., Williams, T., Escutia, C., Brinkhuis, H., 2018. Southern Ocean warming and Wilkes Land ice sheet retreat during the mid-Miocene: Nature. Communications 9 (1), 317.

Sauli, C., Busetti, M., De Santis, L., Wardell, N., 2014. Late Neogene geomorphological and glacial reconstruction of the northern Victoria Land coast, western Ross Sea (Antarctica). Mar. Geol. 355, 297–309.

Sauli, C., Sorlien, C., Busetti, M., De Santis, L., Geletti, R., Wardell, N., Luyendyk, B.P., 2021. Neogene Development of the Terror Rift, Western Ross Sea Antarctica. In: Geochemistry, Geophysics, Geosystems, p. 22.

Solli, K., Kuvaas, B., Kristoffersen, Y., Leitchenkov, G., Guseva, J., Gandjukhin, V., 2007. Seismic morphology and distribution of inferred glaciomarine deposits along the East Antarctic continental margin, 20°E–60°E. Mar. Geol. 237 (3–4), 207–223.

Sugden, D., Denton, G., 2004. Cenozoic landscape evolution of the Convoy Range to Mackay Glacier area Transantarctic Mountains: Onshore to offshore synthesis. GSA Bulletin 116 (7–8), 840–857.

Tinto, K.J., Padman, L., Siddoway, C.S., Springer, S.R., Fricker, H.A., Das, I., Caratori Tontini, F., Porter, D.F., Frearson, N.P., Howard, S.L., Siegfried, M.R., Mosbeux, C., Becker, M.K., Bertinato, C., Boghosian, A., Brady, N., Burton, B.L., Chu, W., Cordero, S.I., Dhakal, T., Dong, L., Gustafson, C.D., Keeshin, S., Locke, C., Lockett, A., O'Brien, G., Spergel, J.J., Starke, S.E., Tankersley, M., Wearing, M.G., Bell, R.E., 2019. Ross Ice Shelf response to climate driven by the tectonic imprint on seafloor bathymetry. Nat. Geosci. 12 (6), 441–449.

Wilson, G.S., Levy, R.H., Naish, T.R., Powell, R.D., Florindo, F., Ohneiser, C., et al., 2012. Neogene tectonic and climatic evolution of the Western Ross Sea, Antarctica — Chronology of events from the AND-1B drill hole. Glob. Planet. Chang. 96–97, 189–203. https://doi.org/10.1016/j.gloplacha.2012.05.019.

Wonik, T., Grelle, T., Handwerger, D., Jarrard, R.D., McKee, A., Patterson, T., Paulsen, T., Pierdominici, S., Schmitt, D.R., Schröder, H., Speece, M., Wilson, T., the ANDRILL-SMS Science Team, 2009. Downhole Measurements in the AND-2A Borehole, ANDRILL Southern McMurdo Sound Project, Antarctica. Terra Antarct. 15 (1), 57–68.

Wright, A.C., Kyle, P.R., 1990. Mount Bird. In: LeMasurier, W.E., Thomson, J.W. (Eds.), Volcanoes of the Antarctic Plate and Southern Ocean, Antarctic Research Series, vol. 48. American Geophysical Union, Washington, D. C., pp. 97–98

Wynn, R.B., Stow, D.A.V., 2002. Classification and characterisation of deep-water sediment waves. Mar. Geol. 192 (1–3), 7–22.